Magnetic Properties of Hexaammineruthenium(III) Trithiocyanate Single Crystals†

Antony B. Blake,[a] Christopher D. Delfs,[a] Lutz M. Engelhardt,[a] Brian N. Figgis,[a] Philip A. Reynolds,*[,a] Allan H. White,[a] Boujemaa Moubaraki[b] and Keith S. Murray[b]

[a] *Department of Chemistry, University of Western Australia, Nedlands, W.A. 6009, Australia*

[b] *Department of Chemistry, Monash University, Clayton, Victoria 3168, Australia*

The crystal structure of monoclinic $(C2/c)[Ru(NH_3)_6][SCN]_3$ has been determined at *ca.* 295 K. The RuN_6 unit is almost of octahedral symmetry, with Ru–N bond lengths of 210.9(4) pm and N–Ru–N angles of 89.9(5)°. The single-crystal magnetic susceptibility has been obtained along the a^*, b and c axes at many temperatures between 2 and 300 K. The ESR g tensor was derived from measurements taken at various angles of rotation about the a^*, b and c axes, at 77 K, giving $g_x = 1.468(3)$, $g_y = 1.929(17)$, $g_z = 2.357(4)$. These data are analysed in terms of an unusually complete crystal-field model in which the parameters are determined with a reliability that is rarely achieved, especially for a second-row transition-metal complex. The axes of the low-symmetry component of the crystal field, as defined by the g tensor, are aligned 12, 23 and 25° from Ru–N directions in the RuN_6 octahedron. This coincidence is probably associated with details of the positions of the hydrogen atoms, or of the SCN^- anions in the unit cell, transmitted through the π electronic structure of the N atoms.

The ground, and lower energy excited states, of paramagnetic systems with both large orbital magnetic moments and large spin–orbit coupling cannot yet be reliably predicted from structural considerations. When the directly co-ordinated ligands are not all the same, or are quite distorted from regular geometry, the angular overlap model is fairly reliable.[1] However, if the primary ligand environment is close to regular octahedral, then the ground state details depend on influences we do not understand. These influences are commonly parametrised by crystal-field models.[2] Such models, as usually implemented, suffer from three defects. First, the true crystal-field symmetry is much lower than that assumed.[3,4] Secondly, insufficient experimental data are then available to fix the large number of crystal-field parameters, leading to doubts about the uniqueness of the model. Thirdly, the crystal-field parameters are empirical and are not obviously connected to the crystal structure.

We would like to understand the connection between structural details and low-lying energies of complexes. We would then be able to predict the electronic states from the crystal structure, either *via* the crystal field or, possibly preferably, directly.

In those paramagnetic systems where orbital magnetic moments are large the magnetic properties are often very anisotropic and very temperature and magnetic field dependent, and very different between similar crystal structures. This provides a long recognised, but rarely successful, means of elucidating the relation between nuclear and electronic structure within crystals by examining optical and magnetic properties.

We hope that, by including several experiments, sufficient information will be available to fix all the parameters of a reasonably full crystal-field model with no *a priori* assumptions about symmetry. The experiments may be optical, bulk and single-crystal magnetic susceptibility and magnetisation measurements, ESR, and polarised neutron diffraction (PND).

† *Supplementary data available* (No. SUP 56939, 5 pp.): magnetic susceptibility measurements. See Instructions for Authors, *J. Chem. Soc., Dalton Trans.*, 1993, Issue 1, pp. xxiii–xxviii.

In the first transition series, we have examined crystals containing hexacyanoferrate(III) and hexaaquairon(II) ions in some detail by these experimental techniques and developed good crystal-field models.[5–7] In the second and third transition series, where spin–orbit coupling is larger, more complicated magnetic effects occur. Examination of a series of crystals containing the same complex ion may be fruitful. However, the large single crystals needed for some of the experiments are not easily grown, particularly for heavy transition-metal complexes, and also the simple symmetrical crystal systems desirable are less common.

An exception may be the simple salts of the low-spin d^5 hexaammineruthenium(III) ion, which is robust and is known to crystallise as salts with many anions.[8,9] However, a crystal structure has been reported only for hexaammineruthenium(III) tris(tetrafluoroborate).[10] The approximate structure of the trichloride may be inferred from the crystal unit cell and ESR data,[11,12] but the full structure is not known.

Accordingly, we have screened a number of hexaammineruthenium(III) salts for ease of crystal growth and suitability of crystal structure.[13] In a previous paper[14] we presented the structure, magnetic susceptibility and ESR results on a cubic salt with a Ru site of O_h symmetry, $[Ru(NH_3)_6]Br[SO_4]$. The cubic symmetry allows the fixing of many of the crystal-independent electronic parameters. The more interesting effects are likely to arise from a lowering in symmetry.

In this paper we present single-crystal X-ray diffraction, ESR and magnetic susceptibility results from $[Ru(NH_3)_6][SCN]_3$. These are enough to construct and, more unusually, test a crystal-field model with no assumptions about the symmetry, other than inversion. We may extend the study to include polarised neutron diffraction when facilities become available.

Experimental

Preparation.—Crystals of $[Ru(NH_3)_6][SCN]_3$ were prepared by metathesis in aqueous solution using hexaammineruthenium(III) trichloride and an excess of ammonium thiocyanate. Large amber parallelopipedal single crystals were produced by slow evaporation from aqueous solution.

Table 1 Atomic fractional coordinates, populations and equivalent isotropic thermal parameters for $[Ru(NH_3)_6][SCN]_3$, [$\bar{U} = (U_{11} + U_{22} + U_{33})/3$ pm^2]

Atom	X/a	Y/b	Z/c	Population	$\bar{U}$
Ru(1)	1/4	1/4	0	1.0	277(1)
S(1)	0.082 30(8)	0.312 0(1)	0.424 2(1)	1.0	624(4)
C(1)	0.124 7(3)	0.350 4(4)	0.561 7(4)	1.0	478(11)
N(1)	0.155 4(3)	0.381 9(4)	0.658 9(3)	1.0	655(12)
N(11)	0.196 8(2)	0.293 9(3)	0.151 8(3)	1.0	404(8)
N(12)	0.194 7(2)	0.041 1(3)	−0.000 5(3)	1.0	421(9)
N(13)	0.110 3(2)	0.317 8(3)	−0.103 5(3)	1.0	411(8)
S(2)	−0.068 6(2)	−0.036 0(2)	0.294 8(2)	0.5	511(6)
C(2)	0.030 5(4)	−0.007 1(7)	0.240 8(5)	0.5	390(10)
N(2)	0.104 0(7)	0.009(1)	0.212 3(8)	0.5	750(30)

Crystal Structure Determination.—*Crystal data.* $[Ru(NH_3)_6][SCN]_3$, $C_3H_{18}N_9RuS_3$, M_r = 377.5, monoclinic, space group $C2/c$, a = 1362.2(6), b = 941.3(3), c = 1174.5(7) pm, β = 103.21(4)°, U = 1.466(1) nm^3, T = 295(2) K, $F(000)$ = 189.9, $D_c(Z = 4)$ = 1.71, D_m = 1.71(1) Mg m^{-3}, μ_{Mo} 1.45 mm^{-1}, crystal morphology {100},{−111}, maximum crystal dimension 0.5 mm, ρ_{max} = 500, ρ_{min} = −700 e nm^{-3}, R = 0.030, R' = 0.034.

Structure solution and refinement. A unique data set was measured at 295 K with a 2θ limit of 75° on an Enraf-Nonius CAD-4 four-circle diffractometer in conventional ω–2θ scan mode. Graphite-monochromated Mo-Kα radiation (λ = 710.69 pm) was used. 3031 Independent reflections were obtained ($|h|$ 0–22, $|k|$ 0–16, $|l|$ 0–19); 2260 with $I > 2\sigma(I)$ were used in a full-matrix least-squares refinement on F_{obs}. After correction for variation in six standards, the data were corrected for absorption analytically (0.70 < transmission < 0.89). No significant decay in the standards was observed. The structure solution was by Patterson methods followed by Fourier difference maps to locate all atoms, including hydrogens. Atomic thermal parameters, except for hydrogen, were allowed to be anisotropic, and statistical reflection counting weights were used. Neutral-atom form factors with anomalous dispersion corrections were used.[15] Computation used the XTAL program system.[16] Conventional residuals on $|F|$, R and R' are quoted in the crystal data list, as well as extrema in the residual electron density (ρ_{max}, ρ_{min}). Extinction was significant but well behaved [Type II, isotropic, g = 1.61(4)]. Non-hydrogen atom coordinates and equivalent isotropic thermal parameters are given in Table 1 and major bond lengths and angles in Table 2.

Additional material available from the Cambridge Crystallographic Data Centre comprises H-atom coordinates, thermal parameters and remaining bond lengths and angles.

Electron Spin Resonance Measurements.—A Bruker ER-100 spectrometer equipped with a liquid-nitrogen Dewar for sample cooling was used at X-band frequency. Single crystals were mounted using Apiezon grease on a flat surface machined in a perspex rod mounted vertically (perpendicular to the applied field), immersed in liquid nitrogen, and attached to a rotating angular scale. The assembly aligns the crystal to within 2° with respect to the magnetic field.

Resonances were observed at 15° intervals with a^*, b and c as crystal rotation axes. As expected from the crystal structure, single resonances were observed with the magnetic field in the ac plane or along b, but two resonances for other directions. Resonant fields were obtained by a least-squares fit of one or two modified Lorentzian derivatives to the digitised experimental traces. The absorption, while broadened due to exchange and relaxation in this undiluted crystal, was still sufficiently narrow to separate the two resonances. The rotation curves were each fitted to the three g parameters, and the three curves used to obtain the three principal g values and the cosines of their directions with respect to a^*, b and c (Table 3). The two choices of assignment of resonance to ion site for the a^* and c data give two solutions for the g tensor. That chosen agrees better with the principal g values estimated from fitting the powder ESR spectrum with a simulated spectrum using the program MONOQF,[17] *viz.* 1.484(5), 2.004(5) and 2.350(5). In the a^*,b,c coordinate system its orientation corresponds to Euler angles[1] of −90(1), 149(1) and −42(1)°.

Table 2 Bond lengths (pm) and angles (°), excluding hydrogen atoms, for $[Ru(NH_3)_6][SCN]_3$

Ru(1)–N(11)	211.3(3)	N(11)–Ru(1)–N(12)	90.4(1)
Ru(1)–N(12)	210.5(3)	N(11)–Ru(1)–N(13)	89.4(1)
Ru(1)–N(13)	210.9(3)	N(12)–Ru(1)–N(13)	89.7(1)
S(2)–C(2)	164.0(7)	S(2)–C(2)–N(2)	174.2(7)
C(2)–N(2)	114(1)	S(1)–C(1)–N(1)	178.0(4)
S(1)–C(1)	162.7(4)		
C(1)–N(1)	116.1(5)		

Table 3 Principal g values and direction cosines (l) with respect to crystal axes

	g_x	g_y	g_z
$\|g\|$	1.468(3)	1.929(17)	2.357(4)
l_{a^*}	0.678(17)	0.629(14)	−0.380(6)
l_b	−0.734(15)	0.585(11)	−0.343(14)
l_c	−0.007(3)	−0.512(5)	−0.859(3)

Magnetic Susceptibility Measurements.—The magnetic susceptibilities of single crystals along a^*, b and c were measured at a magnetic field of 1.0 T from 2 to 300 K using a Quantum Design SQUID magnetometer.[18] After correction for the glue used to attach the crystal to the quartz fibre, and for the diamagnetism of the compound (−238 × 10^{-6} cm^3 mol^{-1}), the molar paramagnetic susceptibilities were obtained. The absolute errors are 0.5% of the measured value; relative errors are lower than this. The complete data are deposited as SUP 56939, and selected values are given in Table 4.

Results

Crystal-field Model.—A general crystal-field model for the ^{2}D term requires 10 parameters if the crystal retains only the inversion symmetry required by the experimental crystallographic site symmetry for the ruthenium(III) ion. Five of these parameters, *viz.* 10Dq, the interelectronic repulsions F_2 and F_4, the spin–orbit coupling constant ζ, and the Stevens orbital reduction factor k, we hope are transferrable between various hexaammineruthenium(III) salts.

The optical spectra of hexaammineruthenium(III) salts show two features which are assigned as the $^4T_g \longleftarrow {}^2T_{2g}$ transition at 23 000 cm^{-1} and $^2T_{1g} + {}^2A_{2g} \longleftarrow {}^2T_{2g}$ at 31 000 cm^{-1}.[19,20] Assuming a ratio of the Racah parameters C/B of 4.0 and ignoring spin–orbit coupling, both sets of workers[19,20] derive values for F_2, F_4 and 10Dq. We introduce a spin–orbit coupling constant, ζ, of 1000 cm^{-1} (see below) and use the crystal-field program suite BFDN[21] to calculate energies within the entire

Table 4 Selected observed and calculated magnetic moments (μ_B) *versus* temperature

	*a**		*b*		*c*	
T/K	Obs.	Calc.	Obs.	Calc.	Obs.	Calc.
2.03	—	1.617	1.447	1.426	1.830	1.826
3.01	—	1.633	1.456	1.437	1.855	1.849
4.51	1.601	1.642	1.467	1.444	1.878	1.860
10	1.609	1.655	1.488	1.458	1.900	1.874
20	1.629	1.671	1.512	1.478	1.916	1.888
60	1.713	1.732	1.593	1.552	1.959	1.940
120	1.836	1.820	1.710	1.658	2.014	2.014
200	1.986	1.931	1.847	1.789	2.085	2.110
300	2.157	2.059	2.000	1.939	2.163	2.222

d^5 manifold. This program accepts as input a crystal-field potential matrix, or some set of parameters which define such a matrix. It requires a set of interelectronic repulsion parameters in the Condon–Shortley scheme. It also accepts a spin–orbit coupling constant, a magnetic field applied in any specified direction relative to the crystal-field axes, and a parameter, k, for scaling the matrix element of orbital angular momentum in the magnetic moment operator. The program constructs a combined operator from the potentials provided and also the complete set of one-electron product wavefunctions which arise from a d^n configuration. For d^5 the number of such functions is 252. It diagonalises the complete set of functions under the operation of the combined operator to yield energies of the perturbed system. Ancilliary programs allow the calculation of magnetic moments and magnetisations, and ESR g values.

By systematically varying the input parameters for BFDN we find a set which reproduces the experimental spectral energy differences. We obtain values of $F_2 = 910$, $F_4 = 66$ and $10Dq = 33\,300$ cm^{-1}. This treatment assigns the first band as from transitions from 22 823 to 23 346 cm^{-1} and the second from 31 161 to 32 111 cm^{-1}, in good agreement with experiment.

For the analysis of the magnetic results, as is common, we reduce the problem from a consideration of the full d^5 manifold to that of only the $^2T_{2g}$ ground term. This removes the need to evaluate the parameters F_2, F_4 and $10Dq$. The magnetic susceptibility and ESR results for $[Ru(NH_3)_6]Br[SO_4]$, with its cubic symmetry ruthenium site, can be used to estimate the only parameters required there, ζ and k, as 1000 cm^{-1} and 0.94 respectively.

Employing as crystal-field parameters the three Euler angles describing the orientation of the low symmetry part of the crystal field relative to the a^*bc axis system and the energies of $3d_{xz}$ and $3d_{yz}$ orbitals relative to that of $3d_{xy}$ as an arbitrary zero, we obtain, as set out before, an excellent and unique fit to the magnetic moments and the ESR g values. The orientation of the low-symmetry components of the crystal field is defined by the Euler angles of the g tensor which are obtained by analysis of the experimental ESR data. We use these Euler angles, and employ the $3d_{xz}$ and $3d_{yz}$ energies as parameters to be determined from g values. We obtain, with $E(3d_{xz}) = -340$ and $E(3d_{yz}) = -170$ cm^{-1}, the fit: $g_x = 1.458$ [obs. 1.468(3)], $g_y = 1.944$ [obs. 1.929(17)] and $g_z = 2.330$ [obs. 2.357(4)].

With no further adjustment, this seven-parameter crystal-field model was used to calculate the magnetisation at 1.0 T along a^*, b and c, and the agreement of the calculated values with experiment is excellent. The results are given in Table 4.

This final seven-parameter crystal-field model predicts the three Kramer's doublets resulting from spin–orbit splitting of the $^2T_{2g}$ term to lie at 0, 1431 and 1627 cm^{-1}. In Table 5 we show the values of $\langle L\rangle$, $\langle S\rangle$ and $\mu\,(=k\langle L\rangle + 2\langle S\rangle)$ along a^*, b and c for the ground state with a magnetic field of 1.0 T along the directions of those axes. The components for the next state (at *ca.* 1 cm^{-1}) arising from the Zeeman splitting of the ground-state Kramer's doublet differ only in sign: the states at 1430 cm^{-1} and above hardly mix with the ground state.

Table 5 Magnetic moment composition of the ground Kramer's doublet at 1.0 T

Component	$\langle L\rangle$	$\langle S\rangle$	$\langle\mu\rangle$
Magnetic field parallel to a^*			
a^*	−0.656	−0.171	0.958
b	−0.099	−0.054	0.202
c	−0.178	−0.082	0.331
Magnetic field parallel to b			
a^*	−0.086	−0.056	0.193
b	−0.627	−0.134	0.861
c	0.002	0.008	−0.017
Magnetic field parallel to c			
a^*	−0.085	−0.052	0.185
b	0.040	0.016	−0.069
c	−0.704	−0.210	1.081

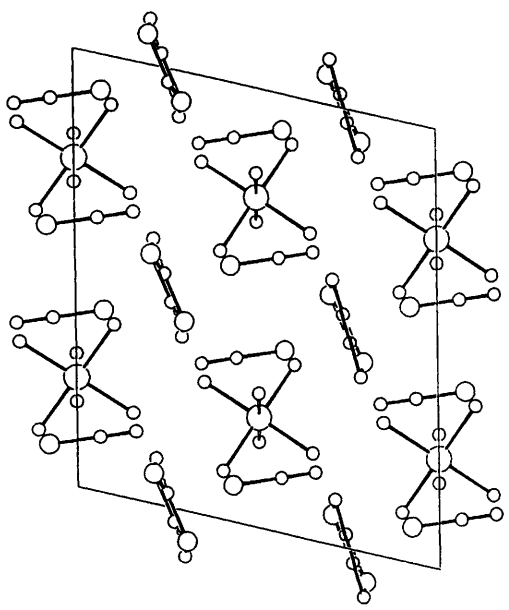

Fig. 1 Unit cell of $[Ru(NH_3)_6][SCN]_3$, projected down b with a^* horizontal, in the plane

The model also predicts that the magnetisation is dominated by the orbital component, and that there is substantial canting of the ionic magnetisation away from the applied field directions of a^*, b and c, by 22, 13 and 10° respectively.

Discussion

Structure.—The structure of $[Ru(NH_3)_6][SCN]_3$ (Fig. 1) may be regarded as composed of hexaammineruthenium(III) ions linked by hydrogen bonding through the thiocyanate anions. This results in an array with eight nearest neighbour Ru···Ru distances at 753.0 pm and four next nearest neighbours at 791.0 pm which gives a distorted face-centred cubic (f.c.c.) arrangement of ruthenium centres. The intramolecular geometry of the ions is as expected except that the S–C–N angle for the disordered thiocyanate ion is 174.2(7)°. This presumably results from an incomplete modelling of the disorder. For our purposes this is not important as we are interested in the hexaammineruthenium(III) sites. The Ru–N bond distances vary from 210.5(5) to 211.3(3) pm, and the N–Ru–N angles are distorted from 90 by only 0.6(1)°. Thus the RuN_6 fragment is very close to octahedral. The hydrogen atom positions, however, cannot be described in any simple way. Their dihedral angles reduce the $Ru(NH_3)_6$ site symmetry to only that of inversion.

Table 6 Polar angles (°) of principal g values and the nearest Ru–N vectors

g_x	89.6(2)	132.7(9)	Ru–N(12^i)	85.5(2)	110.5(2)
g_y	120.8(3)	42.9(9)	Ru–N(13^i)	111.7(2)	19.0(2)
g_z	30.8(3)	42.1(11)	Ru–N(11^i)	22.8(2)	30.4(2)

Symmetry transformation: i $\frac{1}{2} - x, \frac{1}{2} + y, \frac{1}{2} - z$.

Magnetic Behaviour.—In most transition-metal complexes the metal atom is on a site of low symmetry. It was shown experimentally many years ago that the magnetic behaviour in orbitally degenerate situations can only be described using low-symmetry crystal fields.[1,4] Only recently have sufficient data been collected in a few cases[3,5–7] so that the crystal-field or angular overlap[22] model can be tested. For example, for ammonium iron(II) Tutton salt[3] and the Elpasolite Cs_2K-$(Fe(CN)_6]$[5,6] the data have been sufficient and we may be confident that a crystal-field model has been defined which reproduces all the experimental data well.

In this present case of $[Ru(NH_3)_6][SCN]_3$ we have extended this success to the second transition series. Our extensive magnetic data are fitted well by a crystal-field model. Roughly, the ESR experiment tests the eigenvalues of the Hamiltonian of this model, while the magnetic susceptibility and the magnetisation data examine the eigenvectors. Both sets of data are modelled well. We note that the orbital moment is calculated to be about twice the spin moment.

However, we note two things. First, we have a formally ionic model for a second transition-series metal where we expect even more covalence than in the first series. For that series polarised neutron-diffraction experiments have shown that π bonding even in hexaaquametal(II) ions is noticeable.[23] Ammonia is known to have a weaker π interaction with metal ions than has water but, as has been pointed out repeatedly, the ionic crystal-field model still works well. Secondly, both here and in the other two cases, use of the full d-manifold for the crystal-field model produces a noticeably poorer fit to the experimental data than does confining the model to the $^2T_{2g}$ term basis.[5,6,24] We surmise that the excited states are not well described by the ionic crystal-field model. It seems that it is better to omit them completely than to mix in poorly approximated excited states. This observation may well be connected to covalence effects, which, of course, are ignored in the crystal-field model.

The crystal-field parameters deduced are reasonable. Ammonia is known to π bond only very weakly, so the $3d_{xz}$ and $3d_{yz}$ orbital energy parameters of -340 and -170 cm^{-1} are acceptable. The weak π bonding also agrees well with an orbital reduction factor of 0.94, which is little reduced from unity. The spin–orbit coupling constant of 1000 cm^{-1} is also relatively little affected, remaining at about 85% of the free-ion value.[25]

In Table 6 we give polar angles for the principal g values and the nearest set of Ru–N vectors. There is an ambiguity in that we must choose which ion, that at $\frac{1}{4},\frac{1}{4},0$ or at $\frac{3}{4},\frac{1}{4},\frac{1}{2}$ to associate with our g-tensor orientation. We have chosen the set which gives the better agreement between the Ru–N vectors and the principal g value directions. The angles between the vectors and the principal g values, 23, 25 and 12°, are well outside their error limits of less than one degree.

Although the coincidence of the g-tensor axes and the Ru–N vectors is by no means within experimental error, the correlation is obviously high. If the orientation of the g tensor were random then the chance of agreement to within 12 and 23° for two axes is approximately 4%. We included the 48 possible axis combinations in the evaluation of this probability. This coincidence of the g tensor and metal–ligand axes strongly indicates that the low-symmetry crystal field arises from the ammonia molecules. On the other hand, the misalignment is indirect evidence that σ-bonding effects are not the primary source nor would we expect them to be so. It seems that the origin of the low-symmetry component of the crystal field lies in π bonding, and is not simple. It could arise from the symmetry breaking effect of the hydrogen atoms, or by transmission of an influence of neighbouring ions of the crystal through the electronic structure of the ammonia molecules. It is clear that long-range electrostatic effects are not dominant.

Conclusion

The magnetic data presented here provide a good test of the crystal-field modelling process. Probably for the first time, we have shown that such a model can be applied to the second-transition series as a useful summary of experiments, while maintaining a good observation to parameter ratio.

Further progress requires further experiment. We can observe covalence by both X-ray and PND. In particular PND may, by observing how the π magnetisation is delocalised onto the ligands, provide further clues as to the origin of the crystal field. In addition, we can directly observe the canting of the magnetisation, and remove the ambiguity as to which of the two symmestry related ions define the crystal-field parameters. It may also be useful to make *ab initio* predictions of the crystal field, particularly if data on more crystals become available.

Acknowledgements

The authors are indebted to the Australian Research Council (ARC) for financial support. P. A. R. acknowledges support from an ARC Fellowship. A. B. B. is grateful to the University of Hull for study leave.

References

1 M. Gerloch, *Magnetism and Ligand Field Analysis*, Cambridge University Press, Cambridge, 1983.
2 R. L. Carlin, *Magnetochemistry*, Springer-Verlag, Berlin, 1986.
3 R. Doerfler, *J. Phys. C*, 1987, **20**, 2533.
4 M. Gerloch and P. N. Quested, *J. Chem. Soc. A*, 1971, 2307.
5 P. A. Reynolds, C. D. Delfs, B. N. Figgis, B. Moubaraki and K. S. Murray, *Aust. J. Chem.*, 1992, **45**, 1301.
6 C. A. Daul, P. Day, B. N. Figgis, H. U. Gudel, F. Herren, A. Ludi and P. A. Reynolds, *Proc. R. Soc. London, Ser. A*, 1988, **19**, 205; P. Day, C. D. Delfs, P. A. Reynolds, B. N. Figgis and F. Tasset, *Mol. Phys.*, in the press.
7 B. N. Figgis, E. S. Kucharski, P. A. Reynolds and F. Tasset, *Proc. R. Soc. London, Ser. A*, 1990, **428**, 113.
8 K. Gleu, W. Cuntze and K. Rehm, *Z. Anorg. Chem.*, 1938, **237**, 89.
9 K. Gleu and K. Rehm, *Z. Anorg. Chem.*, 1936, **227**, 237.
10 H. C. Stynes and J. A. Ibers, *Inorg. Chem.*, 1971, **10**, 2304.
11 D. Trehoux, D. Thomas, G. Nowogrocki and G. Tridot, *Bull. Chim. Soc. Fr.*, 1971, 78.
12 J. H. E. Griffiths, J. Owen and I. M. Ward, *Proc. R. Soc. London*, 1953, **219**, 526.
13 L. M. Engelhardt, P. A. Reynolds, A. N. Sobolev and A. H. White, unpublished work.
14 P. A. Reynolds, C. D. Delfs, B. N. Figgis, L. M. Engelhardt, B. Moubaraki and K. S. Murray, *J. Chem. Soc., Dalton Trans.*, 1992, 2029.
15 *International Tables for X-Ray Crystallography*, eds. J. A. Ibers and W. C. Hamilton, Kynoch Press, Birmingham, 1974, vol. 4.
16 S. R. Hall and J. M. Stewart, *XTAL System of Crystallographic Programs Version 3.0: Users Manual*, Universities of Western Australia and Maryland, 1990.
17 J. R. Pilbrow and M. E. Winfield, *Mol. Phys.*, 1973, **25**, 1073.
18 Quantum Design Inc., San Diego, CA, 1988.
19 N. Sutin and G. Navon, *Inorg. Chem.*, 1974, **13**, 2159.
20 D. Guenzberger, A. Garnier and J. Dann, *Inorg. Chim. Acta*, 1977, **21**, 119.
21 B. N. Figgis and L. A. Barnes, unpublished work.
22 H. Stratemeier, M. A. Hitchman, R. J. Deeth and R. Hoppe, *J. Chem. Soc., Dalton Trans.*, 1992, 3419.
23 G. S. Chandler, G. A. Christos, B. N. Figgis, D. P. Gribble and P. A. Reynolds, *J. Chem. Soc., Faraday Trans. 2*, 1992, **88**, 1961.
24 C. D. Delfs. Ph.D. Thesis, University of Western Australia, 1991.
25 T. M. Dunn, *Trans. Faraday Soc.*, 1957, **57**, 1441.

Received 10*th September* 1992; *Paper* 2/04871J